

 Open access • Journal Article • DOI:10.2514/1.C032221

## Upset Dynamics of an Airliner Model: A Nonlinear Bifurcation Analysis

— [Source link](#) 

[Stephen J. Gill](#), [Mark H Lowenberg](#), [Simon A Neild](#), [Bernd Krauskopf](#) ...+2 more authors

**Institutions:** [Queen's University](#), [Airbus Group](#)

**Published on:** 24 Dec 2013 - [Journal of Aircraft](#) (American Institute of Aeronautics and Astronautics)

**Topics:** [Upset](#)

Related papers:

- [Application of bifurcation methods to nonlinear flight dynamics problems](#)
- [Dynamics Modeling and Simulation of Large Transport Airplanes in Upset Conditions](#)
- [Nonlinear Analysis of Aircraft Loss of Control](#)
- [Bifurcation Analysis of Nonlinear Aircraft Dynamics](#)
- [AirSTAR: A UAV Platform for Flight Dynamics and Control System Testing](#)

Share this paper:    

View more about this paper here: <https://typeset.io/papers/upset-dynamics-of-an-airliner-model-a-nonlinear-bifurcation-p1wyo3wb24>



Gill, S. J., Lowenberg, M. H., Neild, S. A., Krauskopf, B., Puyou, G., & Coetzee, E. (2013). Upset Dynamics of an Airliner Model: A Nonlinear Bifurcation Analysis. *Journal of Aircraft*, 50(6), 1832-1842.  
<https://doi.org/10.2514/1.C032221>

Peer reviewed version

Link to published version (if available):  
[10.2514/1.C032221](https://doi.org/10.2514/1.C032221)

[Link to publication record in Explore Bristol Research](#)  
PDF-document

Copyright © American Institute of Aeronautics and Astronautics (AIAA)

## University of Bristol - Explore Bristol Research

### General rights

This document is made available in accordance with publisher policies. Please cite only the published version using the reference above. Full terms of use are available:  
<http://www.bristol.ac.uk/red/research-policy/pure/user-guides/ebr-terms/>

# Upset dynamics of an airliner model: a nonlinear bifurcation analysis.

Stephen J. Gill<sup>1</sup>, Mark H. Lowenberg<sup>2</sup> and Simon A. Neild<sup>3</sup>  
*University of Bristol, Bristol, BS8 1TR, UK*

Bernd Krauskopf<sup>4</sup>  
*University of Auckland, Private Bag 92019, Auckland, 1142, New Zealand*

Guilhem Puyou<sup>5</sup>  
*Airbus France, 31060 Toulouse Cedex 03, France.*

Etienne Coetzee<sup>6</sup>  
*Airbus Operations, Airbus, Bristol, BS99 7AR, UK*

Despite the significant improvement in safety linked to the fourth generation of airliners, the risk of encountering upset conditions remains an important consideration. Upset — which may arise from faults, external events or inappropriate pilot inputs — can induce a loss-of-control incident if the pilot does not respond in the correct manner. Any initiative aimed at preventing such events requires an understanding of the fundamental aircraft behaviour. This paper presents the use of bifurcation analysis, complemented by time-history simulations, to understand the flight dynamics of the open loop NASA Generic Transport Model by identifying the attractors of the dynamical system that govern upset behaviour. A number of drivers for potential upset conditions have been identified, including non-oscillatory spirals and oscillatory spins. The analysis shows that these spirals and spins are connected in two-parameter space and that, by an inappropriate pilot reaction to the spiral, it is possible to enter the oscillatory spin.

---

<sup>1</sup> PhD Student, Departments of Aerospace Engineering and AIAA Student Member.

<sup>2</sup> Reader in Flight Dynamics, Department of Aerospace Engineering, and AIAA Senior Member.

<sup>3</sup> Reader in Dynamics and Control, Department of Mechanical Engineering.

<sup>4</sup> Professor of Applied Mathematics, Department of Mathematics, Faculty of Science.

<sup>5</sup> Airbus Operations, Toulouse.

<sup>6</sup> Future Projects Engineer, Airbus Operations.

## Nomenclature

$alt$  = vertical displacement

c.g. = centre of gravity

$C_l$  = body axis rolling moment coefficient

$C_{l_p}$  = rolling moment coefficient due to roll rate

$C_m$  = body axis pitching moment coefficient

$C_n$  = body axis yawing moment coefficient

$C_{n_p}$  = yawing moment coefficient due to roll rate

$C_X$  = x body axis force coefficient

$C_Y$  = y body axis force coefficient (side force)

$C_{Y_p}$  = side force coefficient due to roll rate

$C_Z$  = z body axis force coefficient

$f$  = generic nonlinear function

$lat$  = latitudinal displacement

$lon$  = longitudinal displacement

$p$  = x body axis roll rate

$q$  = y body axis pitch rate

$r$  = z body axis yaw rate

$u$  = x body axis velocity

$V$  = total velocity

$v$  = y body axis velocity

$w$  = z body axis velocity

$X$  = x body axis force

$\mathbf{x}$  = state vector

$Y$  = y body axis side force

$Z$  = z body axis force

$\alpha$  = angle of attack

$\beta$  = angle of sideslip

$\delta_a$  = aileron deflection

$\delta_e$  = elevator deflection

$\delta_r$  = rudder deflection

$\delta_t$  = throttle setting

$\theta$  = pitch angle

$\lambda$  = vector of parameters

$\phi$  = roll angle

$\psi$  = yaw angle

## I. Introduction

The introduction of the fourth generation of airliners has brought a significant improvement in flight safety [1]. However, the risk of encountering upset conditions remains an important consideration. Upset may arise in non-protected aircraft and, potentially, in flight envelope protected aircraft if protection is lost due to faults, external events or inappropriate pilot inputs. This can induce a loss of control event, currently the leading cause of commercial aviation fatalities [2], if the pilot's actions are not effective to recover the upset condition. The activity receiving most attention in attempting to reduce upset events is improved pilot training [3]; other initiatives include fully protected aircraft [4], prediction of upset to improve pilot awareness [5], and automation (from assisted [4] to fully automated [6]) to allow for easier recovery. Whichever solution is being studied, it is important to understand the fundamental aircraft behaviour in these highly nonlinear flight regimes.

In addition to the underlying nonlinear dynamics, upset and upset recovery are also linked to control law characteristics, including envelope protection functions. Today on Airbus aircraft, for example, in the nominal situation ('normal laws') the flight envelope is protected so that abnormal attitudes cannot be reached as a consequence of any of the atmospheric disturbances which have been recorded. However, for very low probability cases combining system fault events (that lead

to a decrease in control law performance) and unusual external perturbations, or in the case of an extraordinary unpredictable external event (e.g. impact damage), the flight parameters may go beyond the limits of the protected envelope. In this case, specific control laws are activated to ensure aircraft recovery. These abnormal attitude control laws essentially consist of direct control on the pitch, roll and yaw axis with very basic and robust stability augmentation in the yaw case. The pilot can then apply classical upset recovery procedures; see for example Ref. [7].

A major objective of the next generation of fly-by-wire aircraft is to further increase safety whilst also improving handling qualities. One potential improvement is to provide the pilot with a higher level of automation even in extreme events, either by introducing advanced manual control laws or by fully automating the recovering procedures (as is already done for some military aircraft [8]). To do so, models and methods for validation and clearance of those new functions are required.

Upset prevention and recovery training is an important tool for reducing loss of control events and will become compulsory for US carriers in 2013 [3]. The industry-developed *Upset Recovery Training Aid* [7] is the most well known document outlining a training programme on upset recovery through piloted simulations. The programme gives pilots knowledge of upset conditions and of basic recovery procedures, practised on full flight simulators, although this document has not yet been widely implemented. The International Committee for Aviation Training in Extended Envelopes (ICATEE) [9] and the Simulation of Upset Recovery in Aviation (SUPRA) [10] programmes also focus their upset prevention and recovery work on piloted simulations. However, the majority of full flight simulators lack the necessary expanded aerodynamic envelope data [11]. Currently, recovery procedure training would require extrapolation of the aerodynamic data from the normal operating envelope and this may result in significant errors and even the mis-modelling of key features of the dynamic response.

Identifying all potential upset scenarios will help to develop the most efficient training approach, which would not be practical by the use of full flight simulators alone. Hence, analytical methods are required to complement the techniques developed for flight simulation. The NASA Aviation Safety Program was created to explore systems associated with the Next Generation Air Transportation System in order to help assure safety. Included in this programme was the development of the

Generic Transport Model (GTM) in order to look at real in-flight upset dynamics and control without the risk attributed to the use of a full scale aircraft; the GTM is a 5.5% dynamically scaled aircraft [12]. Extensive wind tunnel tests were performed on the GTM airframe [11] to create an expanded-envelope aerodynamic data set for use in development of a Matlab Simulink model. It allows the development of control laws that can be implemented in real time on the GTM in-flight model. Much of the GTM research has been on the development of controllers [13, 14] to help prevent upset scenarios and for implementing into the Aircraft Integrated Resilient Safety Assurance and Failsafe Enhancement (AIRSAFE) concept, where resilient control is integrated with flight safety assessment and management; an overview is given in Ref. [15]. However, as research into design of upset controllers is typically not based directly on physical links to the causes of upset and the underlying flight dynamics, these controllers may not work for all possible upset scenarios.

It is the purpose of this paper to provide an improved understanding of the nonlinear flight mechanics that occurs under high angle of attack conditions. To that end, a bifurcation analysis of the GTM, complemented by time-history simulations, is presented. Full bifurcation analysis of civil airliner flight dynamics models is not common practice, although the same approach has been successfully applied to open loop military aircraft models [16–20] and to augmented aircraft dynamics [21–24]. An overview of flight dynamics applications can be found in [25–27]. Bifurcation analysis has already been applied to the GTM in [28, 29]; where a rigorous assessment of the ability to control and regulate an aircraft around bifurcations is provided, with a focus on loss-of-control; the controllability and observability of a closed-loop GTM model is studied, leading to the definition of safe sets in which the aircraft can be positively controlled. This is an important contribution to the topic of upset control relating to bifurcations, including consideration of capacity to recover from upset in the presence failures; it does not attempt to build a comprehensive description of the open-loop flight dynamics in terms of both oscillatory and fixed-point steady states. In Ref. [30], bifurcation analysis was used to classify the different types of behaviour of the open-loop GTM; both elevator and throttle variations were considered, however no specific upset scenarios were discussed. Using these bifurcation diagrams a sequential upset recovery strategy was developed in [31]. Jung [32] implemented bifurcation analysis methods on the VELA1 blended wing body airliner

model and, while it did facilitate a greater understanding of the aircraft’s flight dynamics, it was principally concerned with using control allocation methods to improve handling. While some spin equilibrium solutions were identified, the aerodynamic data was limited to angles of attack of less than  $25^\circ$ . Bifurcation analysis was implemented on the extended envelope version of the SUPRA model [33]. Variation of the flight dynamics in multi-parameter space was investigated; however, as only equilibrium solutions were computed, the existence of other upset attractors, for example periodic orbits, was not addressed.

Murch [34, 35] identified post-stall and spin dynamic modes of the GTM. These spin tests were aimed primarily at discovery of the most accurate forced-oscillation and rotary balance blending function for use in the GTM Simulink model. For this, pro-spin rudder inputs of up to  $\delta_r = \pm 30^\circ$  were used, while other control parameters were zero or at the maximum physical deflection. Therefore, Refs. [34, 35] did not address why the GTM departs into spins and how the characteristics of the spins change as parameters are varied.

Bifurcation analysis is an appropriate method to determine insight into the overall behaviour of the model as it finds and then tracks different types of solutions throughout a parameter range; moreover, the different bifurcations can then be tracked in multi-dimensional parameter space. In this paper, as part of recent initiatives to apply this technique to the open-loop GTM behaviour [30, 31, 36], we present the application of bifurcation analysis to an eighth-order version of the NASA GTM to build an understanding of the underlying flight mechanics. The work identifies possible upset scenarios and, moreover, provides a deeper insight into the complex interactions that govern upset. This can then be focused on problems such as upset prediction and design of prevention/recovery strategies.

## II. Bifurcation and Continuation Analysis

Bifurcation and continuation analysis methods are based on the principles of dynamical systems theory; see, for example, Ref. [37, 38] as entry points to the literature. Solutions are found, and then tracked or *continued* numerically throughout a chosen parameter range in order to generate bifurcation diagrams, which highlight qualitative changes in the system’s dynamic response.



## A. Bifurcation theory

Bifurcation analysis is applied here to an autonomous dynamical system of the general form

$$\dot{\mathbf{x}} = f(\mathbf{x}, \boldsymbol{\lambda}), \quad (1)$$

where  $f$  is a set of  $n$  nonlinear differentiable functions,  $\mathbf{x} \in \mathbb{R}^n$  is the state vector and  $\boldsymbol{\lambda} \in \mathbb{R}^m$  is a vector of  $m$  parameters.

In aircraft open-loop flight dynamics,  $f$  would typically consist of the eighth-order rigid-body equations of motion, see for example Ref. [39] with  $\mathbf{x} = [\alpha, \beta, V, p, q, r, \phi, \theta]$ ;  $\boldsymbol{\lambda}$  may include the control surface inputs (aileron, elevator, rudder, thrust) and/or other parameters, such as centre of gravity location. In numerical bifurcation analysis loci of steady-state solutions are mapped out over a specified range of values of one or more of the parameters, such as elevator deflection; these parameters are referred to as the *continuation parameter(s)*. A one-parameter bifurcation diagram of equilibria (stationary solutions) is generated by setting  $\dot{\mathbf{x}} = f(\mathbf{x}, \boldsymbol{\lambda}) = \mathbf{0}$  and solving the resulting system of equations. Similar continuation (or path-following) methods can be used for finding branches of periodic solutions. Selected state components,  $x_i, i = 1, \dots, n$  are then plotted with respect to the continuation parameter. From these diagrams and using bifurcation theory, bifurcations of the system dynamics can be located and characterised. Various types of bifurcations may arise as parameter values vary, details of which are given in textbooks such as Ref. [37]. Bifurcation theory requires that the model is sufficiently smooth in  $\mathbf{x}$  and  $\boldsymbol{\lambda}$ .

A bifurcation is defined as a qualitative change in the system dynamics as a parameter is varied. Mathematically, a bifurcation of an equilibrium occurs when an eigenvalue of the Jacobian matrix  $Df = \frac{df}{d\mathbf{x}}$  of the system, evaluated at the equilibrium, crosses the imaginary axis. Similarly, for an oscillatory solution, when a Floquet multiplier crosses the unit circle there is a bifurcation of a periodic orbit. In the results presented here, five types of bifurcations are discussed; they are all of codimension one, meaning that they are encountered when a single continuation parameter is varied.

- A saddle node or limit point or fold bifurcation of equilibria occurs when a real eigenvalue of the Jacobian matrix, evaluated at the equilibrium, crosses the imaginary axis. On one side of

the bifurcation point (locally) there are no equilibria and on the other side there are two (for example, one stable and the other unstable).








- A Hopf bifurcation occurs when a complex pair of eigenvalues of the Jacobian matrix, evaluated at the equilibrium, crosses the imaginary axis. Here, the equilibrium changes stability and a periodic orbit is created, which may be either stable or unstable.
- A limit point or fold bifurcation of periodic orbits, which arise when a real Floquet multiplier crosses the unit circle at  $+1$ ; as for equilibria, on one side of the bifurcation (locally) there are no periodic orbits and on the other there are two.
- A period-doubling bifurcation occurs when a real Floquet multiplier crosses the unit circle at  $-1$ . The periodic orbit loses stability while a new periodic orbit with (approximately) twice the period is born.
- A Neimark-Sacker or torus bifurcation is where a periodic orbit loses stability when a pair of complex Floquet multipliers crosses the unit circle and an additional frequency of oscillation is introduced. The result is dynamics on a torus, which may be either periodic (locked) or quasi-periodic.

Numerical continuation methods constitute a set of powerful tools to determine the information necessary to carry out bifurcation analysis. More specifically, they use a predictor-corrector technique to find and then follow or continue curves of equilibria or periodic orbits of the differential equation as roots of an appropriately defined system of algebraic equations. Stability information is computed from eigenvalues of the Jacobian matrix for equilibria and from Floquet multipliers for periodic orbits; bifurcations can be detected and also followed as parameters vary.

## **B. Continuation software AUTO and the Dynamical Systems Toolbox**

A number of continuation software packages are available; this study uses AUTO [40], which is coded in FORTRAN. The package AUTO has been developed in the academic context, where it is widely used. The original version was developed in the 1980's with the latest version, AUTO07P, released in 2007. It has been applied to various aircraft dynamic problems, such as the analysis of

**Table 1 Notation as used in the figures.**

	Stable equilibrium		Hopf bifurcation
	Unstable equilibrium		Torus bifurcation
	Stable periodic orbit		Period doubling bifurcation
	Unstable periodic orbit		

ground dynamics [41], landing gear shimmy [42], landing gear mechanisms [43] and, in addition, to flight dynamics [25] and control [44].

AUTO has the capability, when applied to autonomous dynamical systems, to trace out stationary solutions from an initial starting point to map out the equilibria of the system ( $\dot{\mathbf{x}} = f(\mathbf{x}, \boldsymbol{\lambda}) = \mathbf{0}$ ). While doing this, it is able to detect and label bifurcation points. AUTO also allows the continuation of periodic solutions from Hopf bifurcations or a known starting solution, which allows for the analysis of periodic oscillations. AUTO detects saddle node bifurcations of equilibria, Hopf, saddle node bifurcations of periodic orbits, torus and period-doubling bifurcations, and it can trace the loci of such bifurcation points in two parameters to create a *two-parameter bifurcation diagram*.

In this study, the version of AUTO incorporated into the Matlab Dynamical Systems Toolbox, developed by Coetzee *et al.* [45], was used. This version of AUTO runs the FORTRAN code from the Matlab environment. It uses object orientated coding to set up the problem and then connects to AUTO07P through .mex files. Although computationally more expensive than AUTO07P alone, the use of the Dynamical Systems Toolbox facilitates the setting up of the system in a Matlab or Simulink formulation with access to the associated functions and tools. In the bifurcation diagrams presented here, we use AUTO to depict the stable/unstable equilibria, stable/unstable periodic orbits and bifurcations using the notation given in Table 1.

As is common in numerical bifurcation analysis, we ensured the accuracy of the computations by comparing results with increasingly stringent settings for the tolerances, step size parameters and convergence criteria in the AUTO package; see Ref. [40] for more details. In particular, we ensured convergence to the solution in question to tolerances  $\text{EPSL} = 1\text{e-}006$  and  $\text{EPSU} = 1\text{e-}006$  within  $\text{ITNW} = 5$  corrector steps; moreover, periodic orbits were discretised with  $\text{NCOL} = 4$  collocation points on between  $\text{NTST} = 50$  and  $\text{NTST} = 100$  mesh intervals.

### III. The NASA Generic Transport Model (GTM)

The model used for this research is the Simulink representation of the NASA Generic Transport Model (GTM). Importantly, its wide aerodynamic envelope allows nonlinear analysis at the high angles of attack associated with upset.

#### A. Description of the GTM

The GTM is a 5.5% dynamically scaled civil transport aircraft, which was developed for NASA's Aviation Safety Program [12]. The physical UAV is used for the in-flight analysis of control laws and upset scenarios without the risk associated with using a full scale aircraft. The results presented here are from the Simulink model known as the 'DesignSim'. It implements the nonlinear 6 degree-of-freedom equations of motion for rigid aircraft in atmospheric flight with state vector  $[u, v, w, p, q, r, lat, lon, alt, \phi, \theta, \psi]$ . These equations are defined in, for example, Ref. [39]. The *lat*, *lon* and *alt* states are calculated as angular variables which can then be converted to geographic translations relative to an origin on the earth's surface. Aerodynamic data was taken from extensive wind tunnel tests of the airframe. This gives a flight envelope of  $-5^\circ \leq \alpha \leq 85^\circ$  angle of attack and  $-45^\circ \leq \beta \leq 45^\circ$  angle of sideslip [11]. The aerodynamic data is made up of static and dynamic coefficients in the form of linearly interpolated data tables. Each of the aerodynamic coefficients for the three forces ( $C_X, C_Y, C_Z$ ) and three moments ( $C_l, C_m, C_n$ ) comprises the following contributions:

- static aerodynamic force/moment for zero control surface deflections as functions of  $\alpha$  and  $\beta$ ;
- additional force/moment components from deflecting each of the relevant control surfaces, as function of  $\alpha$ ,  $\beta$  and the deflection angle;
- aerodynamic damping force/moment for each relevant angular velocity, obtained from forced oscillation tests and given as a function of  $\alpha$  and the specific angular rate;
- additional dynamic effects arising from steady state rotation in rotary balance tests, as a function of  $\alpha$ ,  $\beta$  and the rotation rate.

The rotation rates required for the two dynamic contributions (from rotary balance and forced oscillation data) are obtained from  $p$ ,  $q$  and  $r$  using the hybrid Kalviste method [34]. The data tables

are in general nonlinear functions of the given state and control variables. Further nonlinearity exists in the inertial terms, the gravitational acceleration components, and through kinematic coupling. To infer any full scale behaviour, corrections would be required, for example to the aerodynamic coefficients to account for the Reynolds number mismatch. Also, the throttle position, based on the GTM thrust model, is not correlated to full scale as the GTM's thrust to weight ratio is larger than that of a typical airliner. Note that the DesignSim model is not intended to represent a full-scale aircraft: the data was generated for the sub-scale vehicle for the Reynolds numbers at which it was tested, and the modeling uncertainties — which are potentially larger at higher incidences than in the conventional flight envelope — are not quantified.

## B. Implementation of the GTM

The Simulink based model was connected to AUTO within the Dynamical Systems Toolbox [45]. The linear interpolation of tabular aerodynamic data resulted in an insufficiently smooth system for numerical continuation and a number of alternative interpolation methods were investigated. Ultimately, the Simulink interpolation n-D block running cubic spline interpolation was implemented as it creates smooth data and was quicker to set up than, for example, fitting multivariate orthogonal functions [46]. No unacceptable overfitting was observed in these spline representations of the data tables.

For analysis of flight mechanics, the  $[u, v, w]$  body axes states used in the GTM DesignSim equations of motion are not as intuitive as the wind axes velocities  $[\alpha, \beta, V]$ . These states are calculated in the GTM as auxiliary variables, but, when periodic orbits are computed, the minimum and maximum values of  $[\alpha, \beta, V]$  are not readily available. Therefore, in our implementation, the translational equations of motion were rewritten directly in wind axes form using expressions taken from [47].

For the bifurcation analysis presented here, the GTM is reduced to an eighth-order model. To implement this eighth-order model, the feedbacks of the unused states  $[lat, lon, alt, \psi]$  were terminated and replaced by constant values (the initial conditions). This results in the reduced system with state vector  $[\alpha, \beta, V, p, q, r, \phi, \theta]$ . With this modification the model still captures the

full dynamics of the system in body axes, except that, since altitude is fixed, the influence on the aerodynamic loads of varying air density is neglected. However, this effect is negligible in terms of the time scale associated with stability and control studies. For generating flight trajectories of the GTM in the earth axes, the full twelfth-order system is used (with  $lat$  and  $lon$  the translations relative to the position at  $t = 0$ ). Furthermore, the actuators dynamics were not considered in the computations since this has no effect on open-loop solutions: at each of the continuation run points the control surface deflections were fixed. This reduced the complexity of the model, thus allowing a faster runtime.

#### IV. Bifurcation analysis of the GTM aircraft

The results presented in this section are for the eighth-order open loop representation of the NASA GTM aircraft (referred to here as GTM\_8ol) with state vector  $[\alpha, \beta, V, p, q, r, \phi, \theta]$  and centre of gravity at the nominal location of 24% mean aerodynamic chord. The starting point of the continuation was calculated using the trim function supplied with the GTM at  $\alpha = 3^\circ$  and flight path horizontal, where  $V = 47.34$  m/s and  $alt = 243$ m (800ft). This gave initial state and control parameter vectors of:

$$\mathbf{x} = \begin{bmatrix} \alpha & \beta & V & p & q & r & \phi & \theta \end{bmatrix}^T = \begin{bmatrix} 3^\circ & 0^\circ & 47.34m/s & 0^\circ & 0^\circ & 0^\circ & 0.01^\circ & 3^\circ \end{bmatrix}^T$$

$$\boldsymbol{\lambda} = \begin{bmatrix} \delta_a & \delta_e & \delta_r & \delta_t \end{bmatrix}^T = \begin{bmatrix} -0.004^\circ & 2.58^\circ & 0.009^\circ & 22.05\% \end{bmatrix}^T$$

The trim aileron and rudder were non-zero due to the asymmetry in the aerodynamics and the alignment of the engines. The aerodynamic asymmetry was observed in the wind tunnel data upon which the model is built. Its source is not well understood: Ref. [11] suggests that it may arise from wing stall or flow fields emanating from the forebody. There is ongoing research to establish whether wing stall is the probable cause for roll asymmetry [48]. The very small difference in alignment angles between the two engines was incorporated into the engine model on the basis of measurements from the 5.5% scale flight vehicle. However, that aileron and rudder deflections are very small indicates that at  $\alpha = 3^\circ$  the asymmetry is also small. To initiate the study, the elevator deflection angle,  $\delta_e$ , was the chosen continuation parameter, so as to emulate the pilot pulling back or pushing forward on the stick with constant throttle, while not altering the ailerons and rudder. The continuation

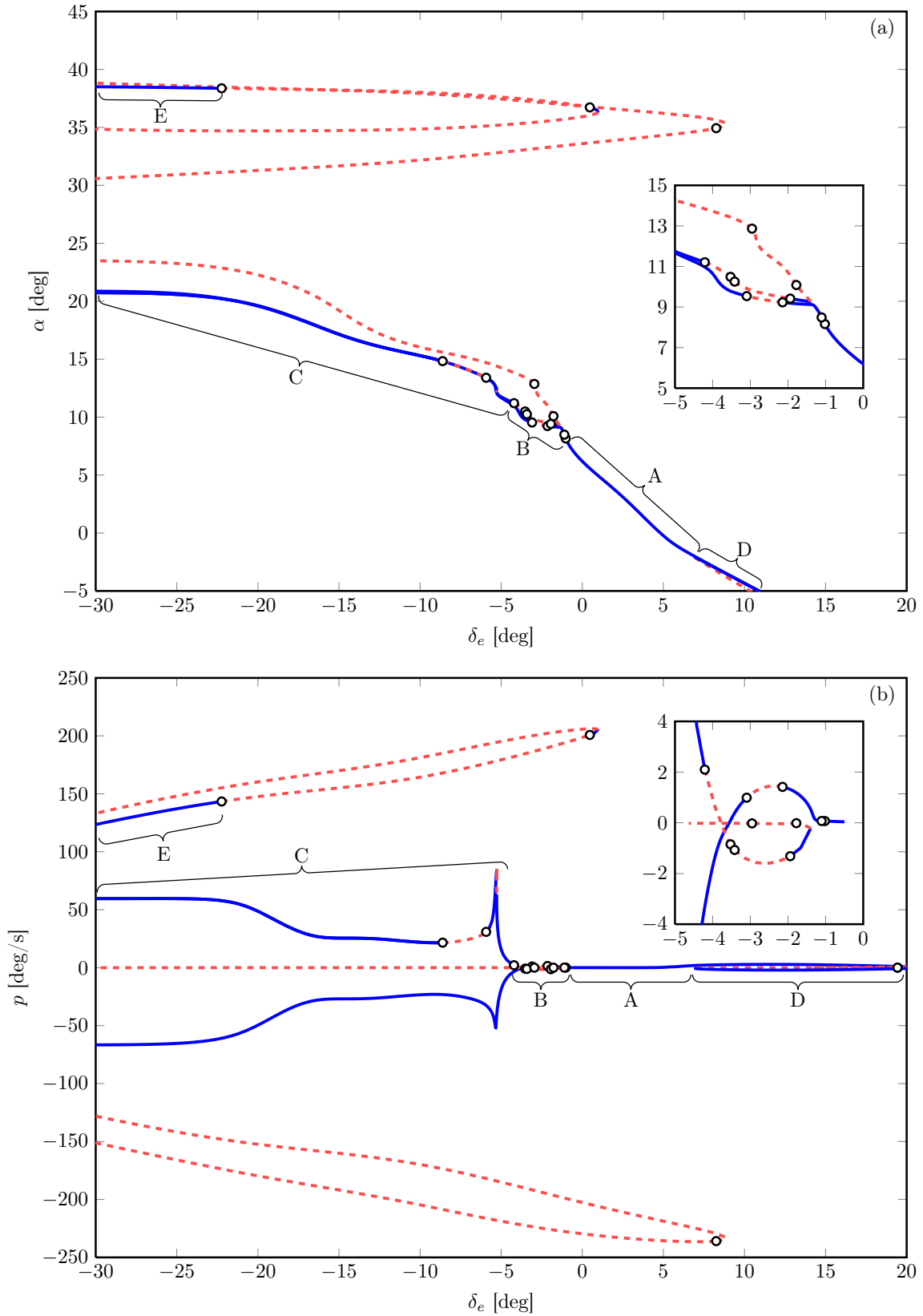


**Fig. 1** One-parameter bifurcation diagrams in elevator deflection,  $\delta_e$ , of equilibrium solutions for GTM\_801 showing angle of attack  $\alpha$  (a) and roll rate  $p$  (b); here  $\delta_a = -0.004^\circ$ ,  $\delta_r = 0.009^\circ$  and  $\delta_t = 22.05\%$ . The insets show enlarged views of regime B.

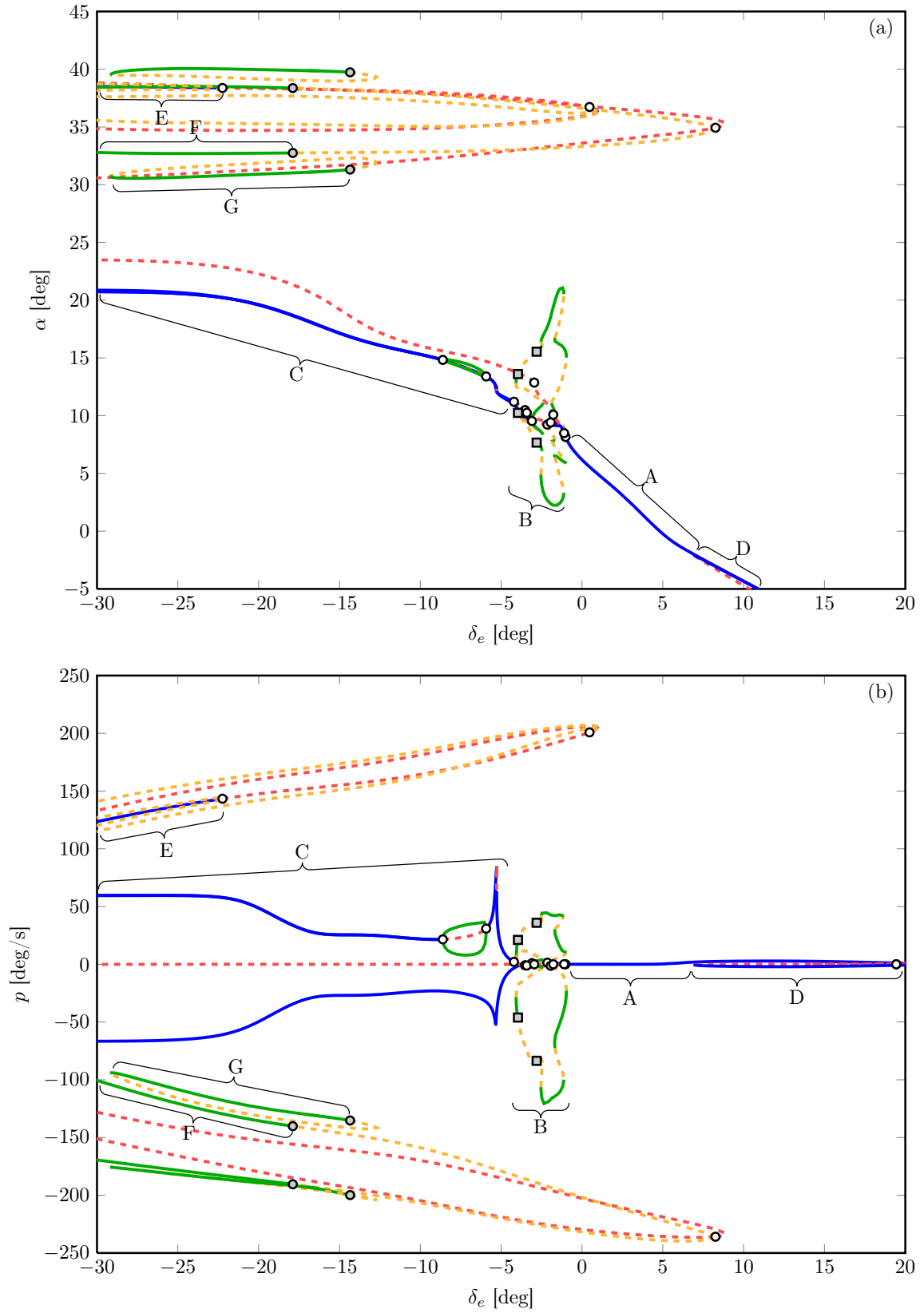


**Fig. 2** One-parameter bifurcation diagrams in elevator deflection,  $\delta_e$ , of equilibria and periodic solutions for GTM\_80l showing angle of attack  $\alpha$  (a) and roll rate  $p$  (b); here  $\delta_a = -0.004^\circ$ ,  $\delta_r = 0.009^\circ$  and  $\delta_t = 22.05\%$ .



was run in both positive and negative directions from the initial point of  $\delta_e = 2.58^\circ$  and the results were computed beyond the physical elevator limits of  $-30^\circ \leq \delta_e \leq 20^\circ$  to be able to detect steady state solutions that leave and re-enter the realistic parameter range.

Figure 1 shows a one-parameter bifurcation diagram in  $\delta_e$  for the states  $\alpha$  and  $p$  showing equilibrium solutions only. The insets in panels (a) and (b) show respective enlargements of the bifurcation diagram for small negative  $\delta_e$ . Figure 2 builds on this information by including the periodic solutions. In Figs. 1 and 2 the solutions lie in two distinct regions: the first at low to medium angles of attack ( $\alpha \approx -5^\circ$  to  $25^\circ$ ) and the second at higher angles of attack ( $\alpha \approx 30^\circ$  to  $42^\circ$ ). In these two regions we classify the different types of dynamics into seven regimes, labelled A—G and denoted in table 2. The regions are linked outside the physical limits of the elevator and were located by applying the continuation algorithm well beyond the realistic parameter range. The behaviour in each of these two regions is now discussed individually; subsequently in section V we present how these two branches are connected within the physical elevator range by using rudder deflection,  $\delta_r$ , as the continuation parameter.

**Table 2 Dynamic regimes.**

Symbol	Type of Dynamics	$\alpha$ range
A	Stable trimmed symmetric flight	$-2^\circ$ to $8^\circ$
B	Low frequency oscillations	$2.2^\circ$ to $21^\circ$
C	Steady steep spiral	$10.5^\circ$ to $20.9^\circ$
D	Inverted spiral	$-5^\circ$ to $-2^\circ$
E	Steady steep spin	$30.5^\circ$ to $38.8^\circ$
F	Period-one oscillatory steep spin	$32.7^\circ$ to $38.5^\circ$
G	Period-three oscillatory steep spin	$30.8^\circ$ to $40^\circ$

### A. Low $\alpha$ behaviour

At the starting point of the continuation run ( $\alpha = 3^\circ$ ), GTM\_8sol exhibits stable symmetric flight. As the elevator deflection decreases (i.e. the pilot pulls back on the stick), angle of attack initially increases with roll rate remaining at zero. This dynamic regime, labelled A in the  $\alpha$  range

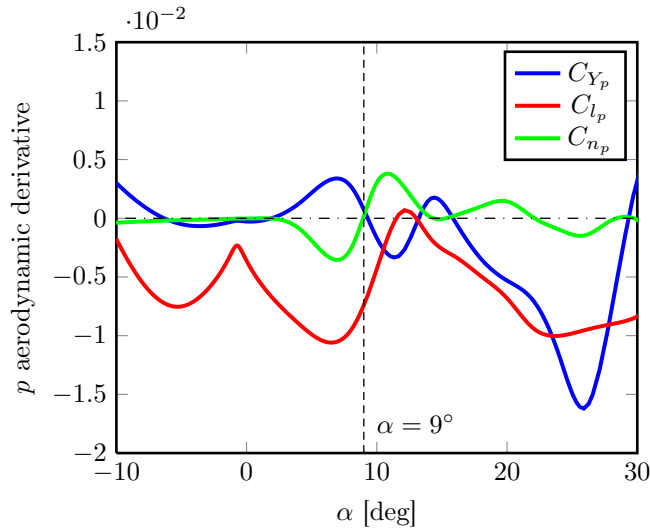


**Fig. 3** Aerodynamic derivatives with respect to  $p$  versus  $\alpha$ , with the derivatives taken around the point  $\beta = 0^\circ$ .

of  $-2^\circ$  to  $8^\circ$  in Fig. 1, can be considered as the normal trimmed symmetric flight condition. As the elevator deflection decreases past  $\delta_e \approx -1^\circ$ , where  $\alpha \approx 8^\circ$ , GTM\_80l enters the regime of dynamics labelled B where predominantly longitudinal oscillations exist, which can be related to an unstable phugoid mode. These longitudinal oscillations arise from the Hopf bifurcations which exist in B. Within this segment, as elevator deflection decreases further through  $\delta_e \approx -1.3^\circ$  and  $\alpha = 9^\circ$  the spiral mode loses stability, leading to a bifurcation from the near-symmetric stable solution such that two strongly non-symmetric branches of equilibrium solutions appear; at angles of attack beyond this point, the spiral mode is unstable on the near-symmetric branch. Note that this coincides with the aerodynamic derivatives  $C_{Y_p}$  and  $C_{n_p}$  changing sign; see Fig. 3. At angles of attack slightly beyond the onset of asymmetry, Hopf bifurcations occur; these are triggered by changes in stability of the phugoid mode although the resulting oscillations involve coupled longitudinal and lateral-directional motions. The period of these orbits is long ( $\approx 30s$  for the subscale aircraft) and time histories have shown that these orbits are weak attractors. Hence the oscillations in regime B cannot be considered as upset scenarios and are not discussed further here. More detail on this flight regime of the GTM can be found in [36].

The asymmetry grows as elevator deflection is further decreased and at  $\delta_e \approx -4^\circ$  the aircraft enters regime C where large magnitude roll departure is experienced; see Fig. 1b. Stable equilibrium

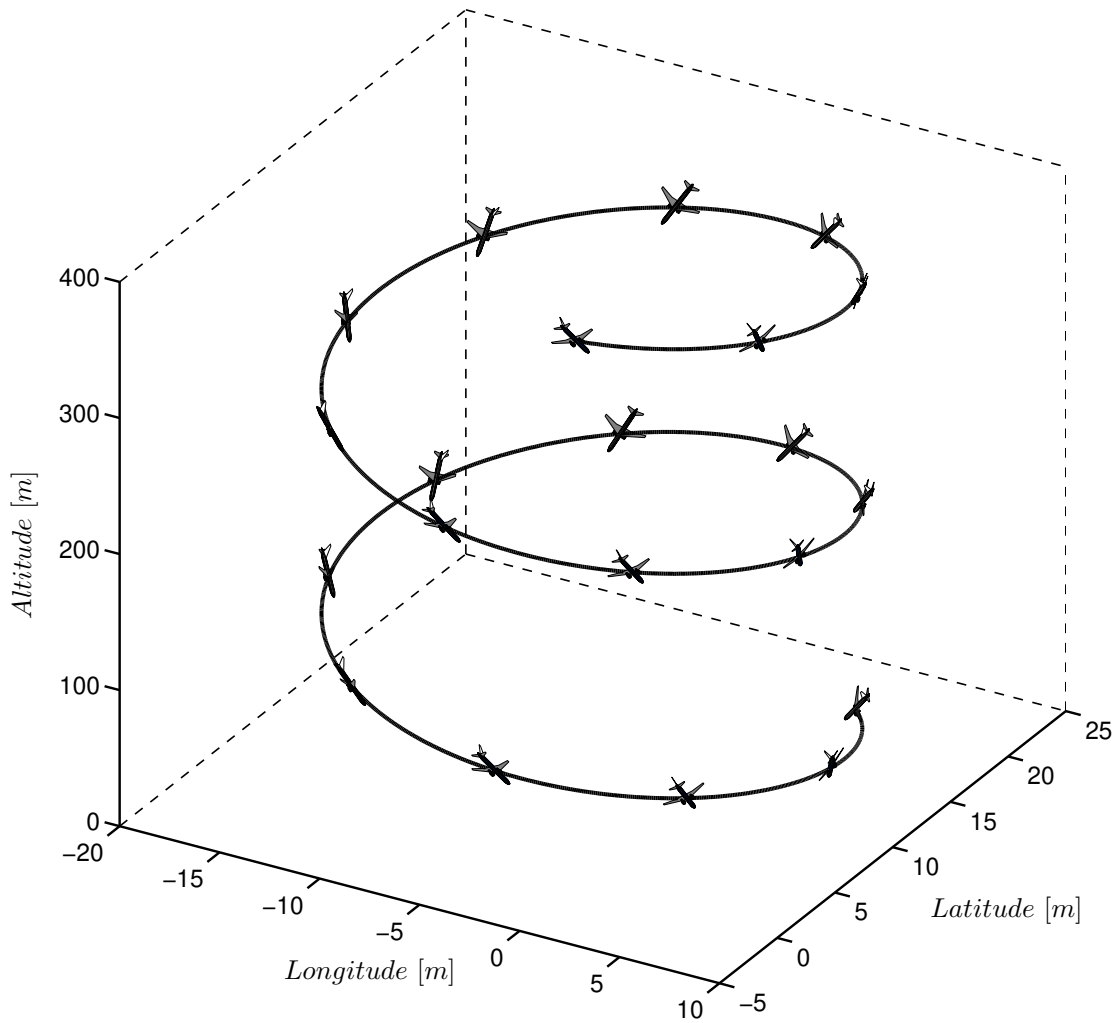


**Fig. 4** Trajectory of the ‘steep spiral’ of regime C, for  $\delta_e = -30^\circ$ .

branches exist to both sides of the straight and level equilibrium, although, as the aerodynamics are asymmetric, GTM\_801 is ‘likely’ to depart to the left, i.e. with negative  $p$ . This results from the equilibrium branch representing departure to the left being connected to A through B (see magnified views in Fig. 1). The equilibrium branch representing departure to the right is actually disconnected from A and reaches a limit point bifurcation where the solution folds back, becoming the unstable equilibrium where  $p \approx 0^\circ/s$ . (We remark that if GTM\_801 were perfectly symmetric then it would ‘prefer’ neither side and any lateral instability of the zero  $p$  branch would arise at what is known as a pitchfork bifurcation [37].) Whether the aircraft spiral develops to the left or the right will in practice depend on the nature of the disturbance and/or transient dynamics. As shown in Fig. 1 these equilibrium branches of dynamic regime C do not converge on the straight and level

flight branch within the physical elevator range; hence, GTM\_8ol will stay on one of the two spiral branches up to and including full aft column at  $\delta_e = -30^\circ$ . Regime C represents stable steady-state equilibria in the bifurcation diagram in Figs. 1 and 2. Fig. 4 is a trajectory plot from the full twelfth-order model time history; note that in this and subsequent trajectory plots, the aircraft is depicted approximately to scale with respect to latitude and longitude. The trajectory shows that regime C represents undesirable steep helical spirals. These *steep spirals* can be considered as upset conditions, although as can be inferred from Fig. 1, GTM\_8ol can be recovered easily by reducing angle of attack to below that at which the spiral branches arise, which may be achieved by simply pushing forward on the stick. This matches the advice for stall recovery given in [7]. The ability to find and quantify branches like the steep spirals highlights the advantage of continuation and bifurcation analysis over linear methods, which would find the change of stability but would not easily find the stable spiral branches.

A slight lateral instability exists at low angles of attack ( $\alpha \leq 0^\circ$ ), labelled D in Figs. 1 and 2. For this constant-thrust bifurcation diagram, the flight velocity peaks at unrealistically high values at small negative angles of attack, accompanied by increasingly negative pitch angle, until the aircraft is in fact inverted. Thus, although regime D may be considered an inverted spiral, it is not representative of realistic conditions and is hence not considered further here.

## B. High $\alpha$ behaviour

At higher angles of attack, in the range  $30^\circ < \alpha < 40^\circ$  in Fig. 1 and 2, additional solutions exist. First of all, there are branches of equilibria that span  $-30^\circ < \delta_e < 1^\circ$  for positive roll rate and  $-30^\circ < \delta_e < 8^\circ$  for negative roll rate. All these negative roll rates are unstable, whilst there is a considerable region of stable equilibria with positive roll rates. These differences arise from the asymmetries in the model: the fundamental changes in inertial and aerodynamic force balance in the left- and right-hand spins have not been identified but it is evident that they do affect the nature of the resulting spin branches — including their local stability — just as they do at lower  $\alpha$ . These stable equilibria correspond to steady spins which we refer to as dynamic regime E. (Note that there is also a tiny region of stable spins near  $\delta_e = 1^\circ$  but this is not of practical relevance.) Observation

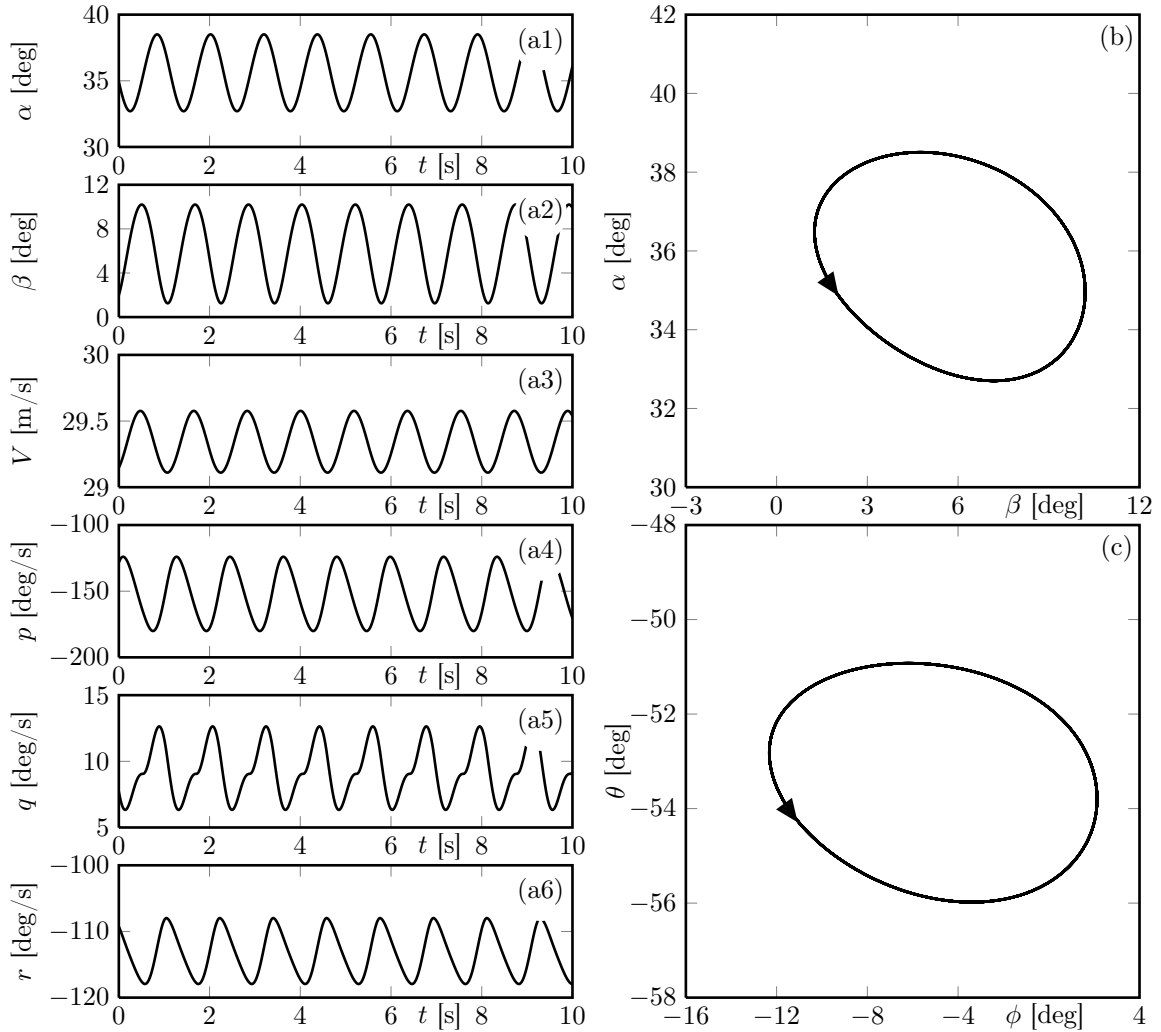


**Fig. 5** Time history of the period-one oscillatory spin of regime F for  $\delta_e = -24^\circ$ , showing time traces of:  $\alpha, \beta, V, p, q$  and  $r$  (panels a1—a6). Panels (b) and (c) show the periodic orbit in the  $(\beta, \alpha)$  and  $(\phi, \theta)$ -planes, respectively.

of time history responses in the region of regime E showed that it has a small region of attraction; thus this steep spin equilibrium branch does not play a significant role in the upset dynamics for the chosen c.g./throttle setting. Although in the range  $30^\circ < \alpha < 40^\circ$  the majority of equilibria are unstable and do not in themselves provide a steady spin, these solutions may influence responses in this region and this has the potential to cause chaotic behaviour. Importantly there exist three Hopf bifurcations in the valid parameter region, at  $\delta_e = 0.47^\circ$ ,  $\delta_e = 8.26^\circ$  and  $\delta_e = -22.2^\circ$ ; all occur at  $\alpha > 30^\circ$ . Continuation of the periodic orbits from the Hopf bifurcations at  $\delta_e = -22.2^\circ$

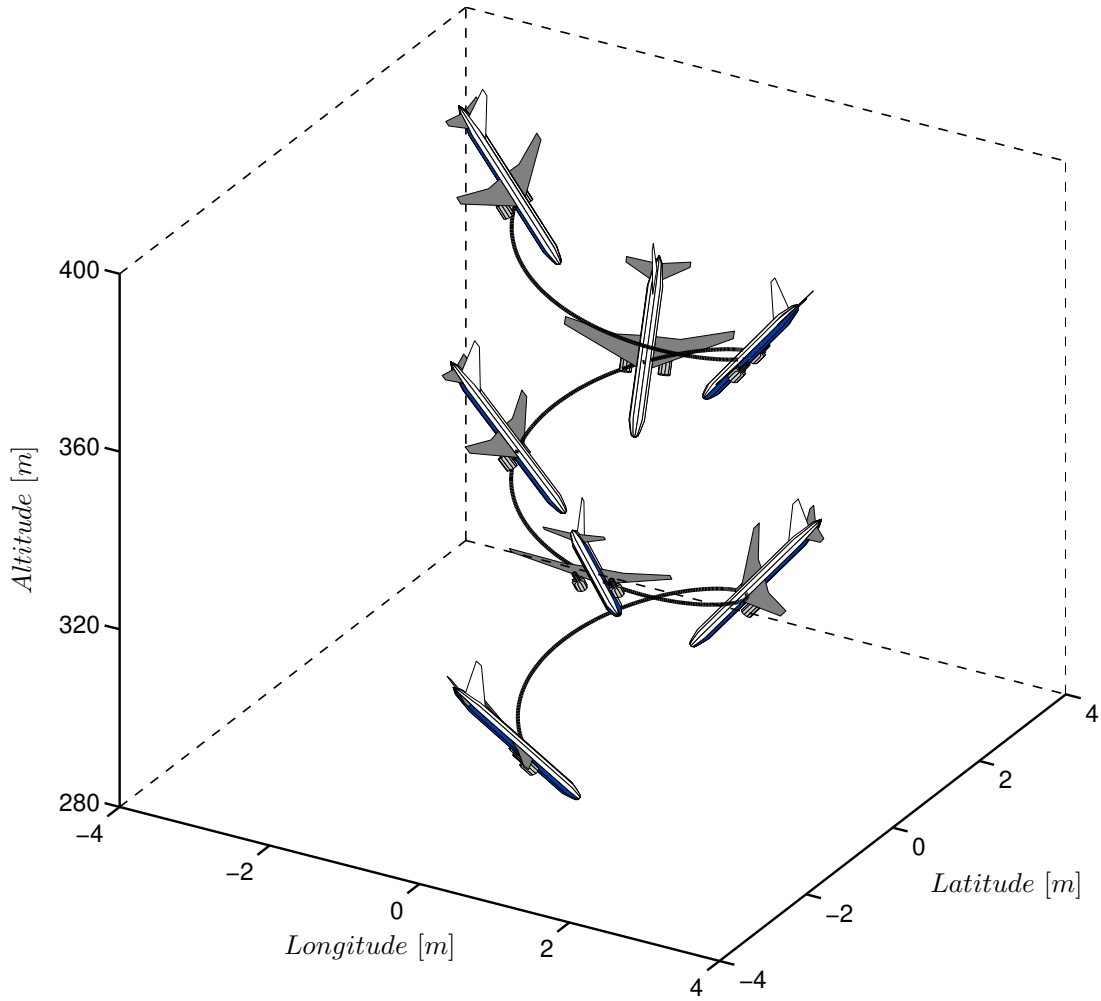


**Fig. 6** Trajectory of the period-one oscillatory spin of regime F for  $\delta_e = -24^\circ$ .

and  $0.47^\circ$  show them to be unstable throughout the valid parameter range. Of more significance is the continuation of the periodic orbit from the Hopf bifurcation at  $\delta_e = 8.26^\circ$ , which is initially unstable but then bifurcates to a stable periodic orbit via a torus bifurcation at  $\delta_e = -17.9^\circ$ . The stable periodic orbit in regime F in Fig. 2 is significant as here the average angle of attack is  $\alpha \approx 35^\circ$  with high magnitude roll and yaw rates. This periodic orbit is shown in the time history and phase portrait plots for  $\delta_e = 24^\circ$  in Fig. 5. These dynamics in regime F may be regarded as an oscillatory steep spin with a flight path angle of  $\gamma \approx -89^\circ$ . The trajectory plot of this periodic orbit, in Fig. 6, shows this oscillatory spin to be much tighter than that of the steep spiral in Fig. 4. The oscillatory spins shown for the GTM in Ref. [34] also had an average angle of attack of approximately  $35^\circ$ : although non-zero rudder and aileron deflections were used in [34], it is typically angle of attack

that dominates aerodynamic nonlinearity so that this similarity is not unexpected. Figure 2 shows that this spin mode does exist at  $\delta_a \approx \delta_r \approx 0$  and  $\delta_t = 22.05\%$ .

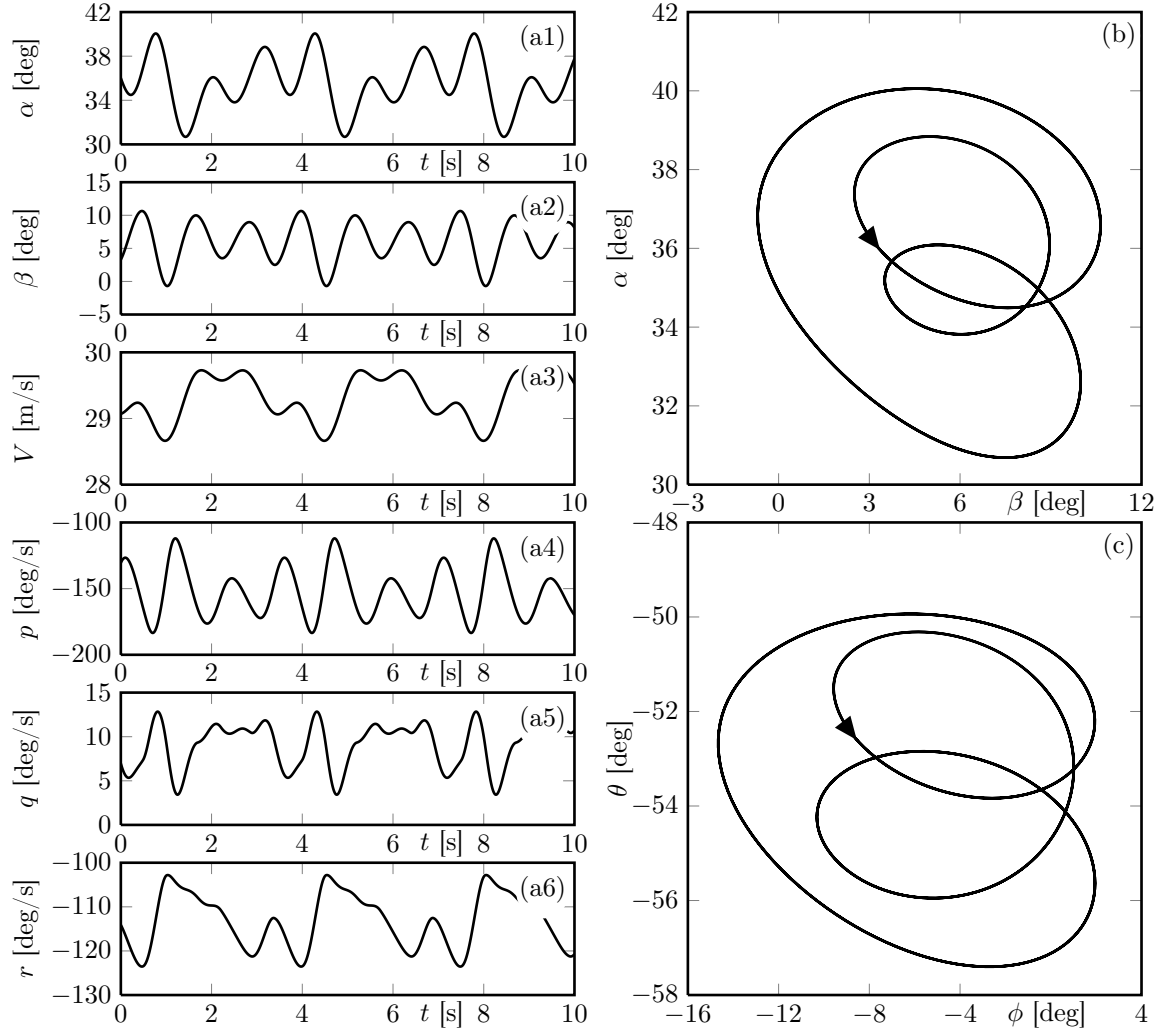


**Fig. 7** Time history of the period-three oscillatory spin of regime G for  $\delta_e = -24^\circ$ , showing time traces of:  $\alpha, \beta, V, p, q$  and  $r$  (panels a1—a6). Panels (b) and (c) show the periodic orbit in the  $(\beta, \alpha)$  and  $(\phi, \theta)$ -planes, respectively.

A second stable periodic orbit was also identified in the high angle of attack region; see regime G in Fig. 2. This solution exists on an ‘isola’ (a closed curve that is not connected to the other bifurcation curves); it was discovered by running a time history beyond the torus bifurcation on the orbit of regime F at  $\delta_e = -17.9^\circ$ . At this point this periodic orbit is no longer stable and the GTM\_8ol is attracted to the periodic orbit of regime G. Figure 7 shows that regime G represents

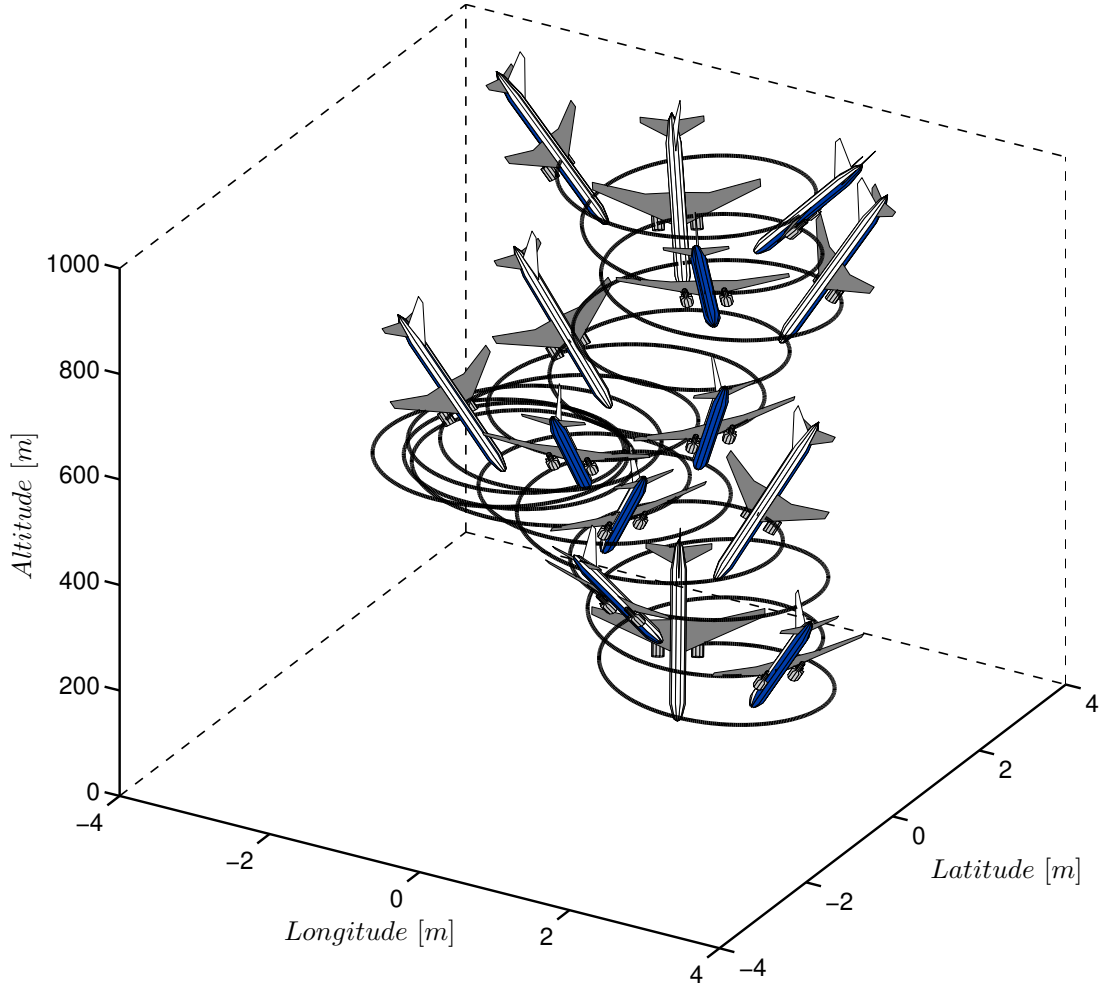


**Fig. 8** Trajectory of the period-three oscillatory spin of regime G for  $\delta_e = -24^\circ$ .

a more violent oscillation than that in regime F. Specifically, Fig. 7 shows that it is a period-three periodic orbit, indicated by the fact that it has three amplitude maxima and minima. The trajectory plot of a time history of this period-three orbit in Fig. 8 shows that it also constitutes a very tight spin mode.

The comparison of the ground-tracks of the steep spiral, the period-one periodic orbit and the period-three periodic orbit in Fig. 9 shows that there is a substantial difference in these trajectories in both scale and complexity. The steep spiral in Fig. 9a is a perfect circle, as this is a steady state solution of the eighth-order system defined in body axes coordinates; therefore, although it is spiralling, this solution has constant angular rates and angular displacement relative to the trajectory so that the radius of the spiral in the latitude-longitude plane is constant. The two



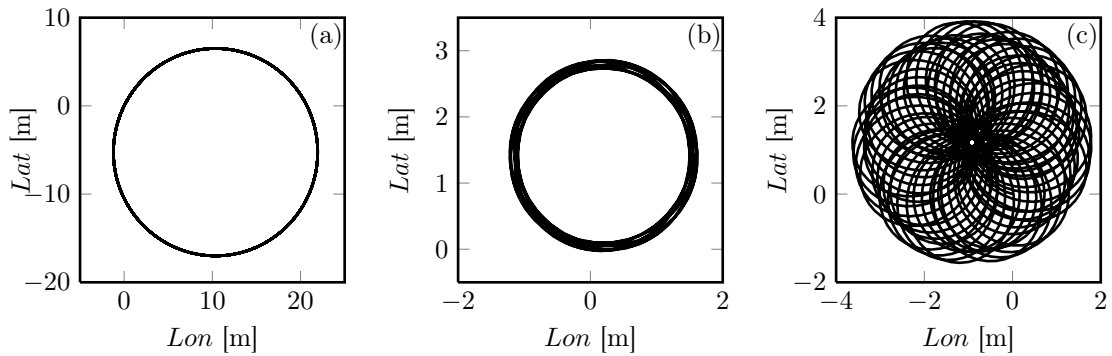


**Fig. 9** Ground-tracks for the steep spiral of regime C for  $\delta_e = -30^\circ$  (a), the period-one periodic orbit of regime F for  $\delta_e = -24^\circ$  (b), and the period-three periodic orbit of regime G for  $\delta_e = -24^\circ$  (c).

periodic orbits, however, do not have constant angular rates and, therefore, the radius of the spin also oscillates. In the earth axis these appear as oscillating helices; see Figs. 6–8. The extent of the ‘wander’ of the ground-track differs depending on the nature of the oscillatory solution, as the wander depends on the change of the radius during one period of the periodic orbit. The period-one periodic orbit of regime F in Fig. 9b shows little wander, however, the period-three orbit of regime G in Fig. 9c exhibits far more noticeable wander. As these limit cycles both lose stability at torus bifurcations it can be seen from Fig. 2 that by reducing elevator deflection beyond these torus points and towards regime A the GTM will recover to straight and level flight as no other stable attractors exist in the high angle of attack region. This procedure is the same as that given for recovery from the steep spiral in section IV A although care must be taken that the transient response of the recovery would not cause structural damage to the airframe. An example of this recovery is given in Fig. 11 of [36].

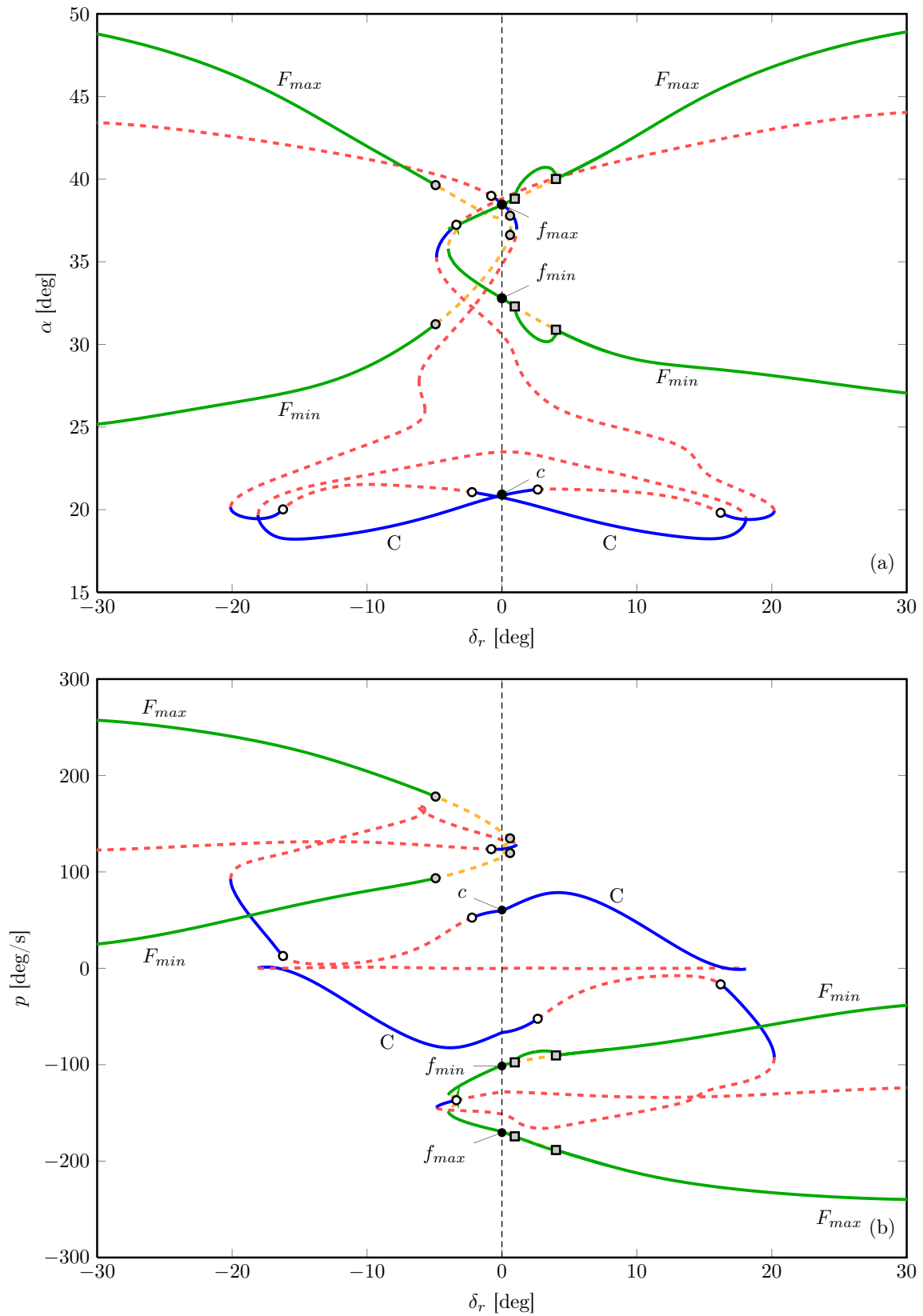
### V. Transition from spiral to spin solutions

As mentioned in section IV, in elevator deflection alone the spiral and spin modes are only connected outside the physical elevator range, inferring that only a large external perturbation might transfer the GTM from the steep spiral to the oscillatory spins of regimes F and G. However, these solutions may still be connected within the physical  $\delta_e$  range when other parameters vary. To investigate this, rudder deflection  $\delta_r$  is selected as the continuation parameter and elevator deflection

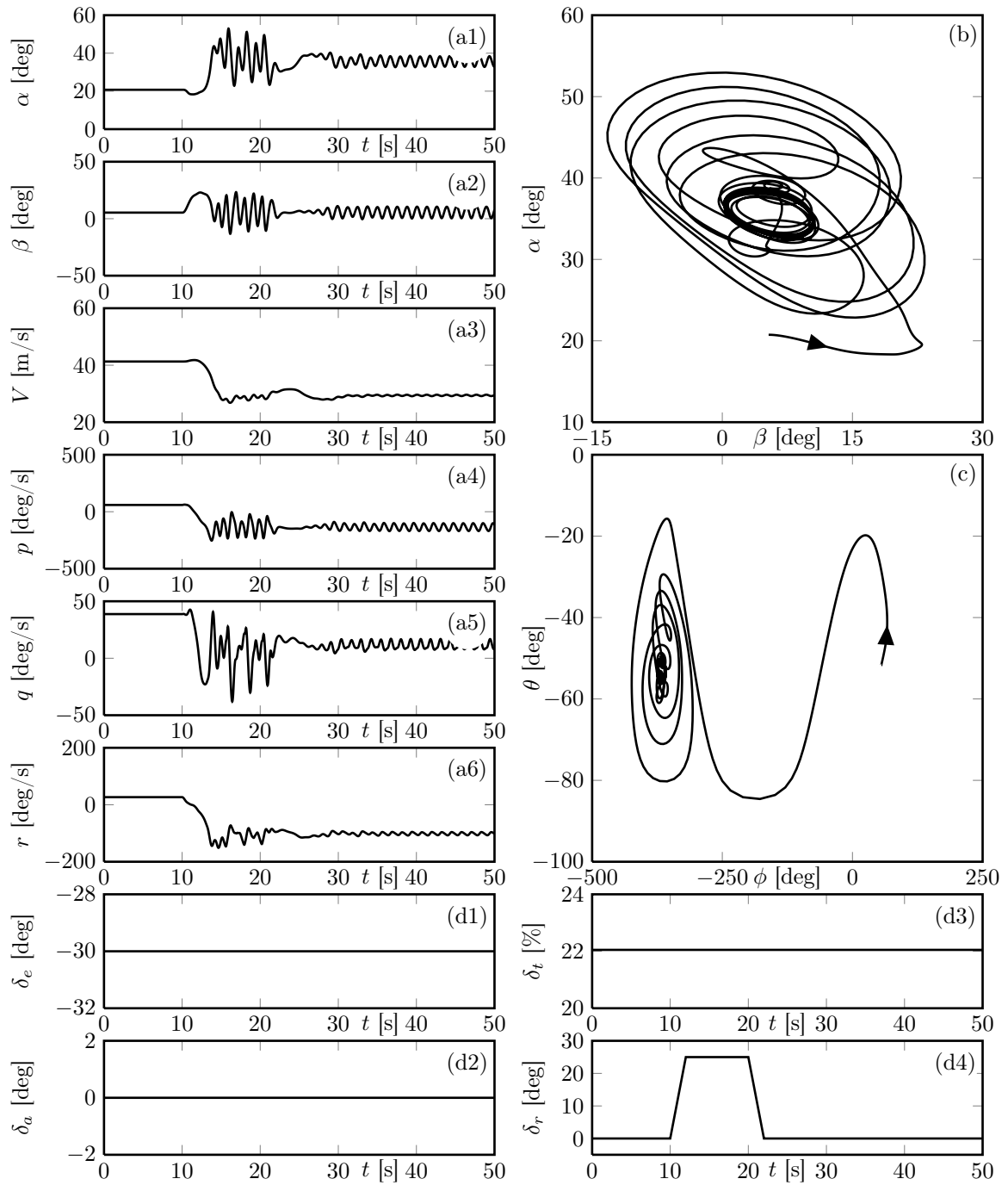
kept at a constant  $\delta_e = -30^\circ$ , while aileron and throttle are retained at their original trim values.

Figure 10 shows the  $\alpha$  and  $p$  projections of this one-parameter bifurcation diagram. At  $\delta_r = 0.009^\circ$ , the solutions on the dotted line are the same solutions as shown at the left-hand boundary of Fig. 2 where  $\delta_e = -30^\circ$  (here  $c$  represents the solution on regime C,  $f_{min}$  and  $f_{max}$  are the minimum and maximum values of the orbit on regime F). The two stable equilibria at  $\alpha \approx 21^\circ$  are the steep spiral equilibria of regime C, and the stable periodic orbit at  $32 \leq \alpha \leq 39^\circ$  is the periodic orbit of regime F. We note that the steep spiral and oscillatory spin solutions are indeed connected within the physical rudder deflection limits for  $\delta_e = -30^\circ$ . More specifically, Fig. 10 shows that, once rudder deflection is taken beyond  $\delta_r \approx \pm 20^\circ$ , the GTM\_sol will enter a large oscillatory spin to either the left or right as no other stable attractors exist beyond these points. Figure 10 also shows that, once in a spin to the right (i.e. with positive lateral variables), if the rudder deflection is then returned to zero the periodic orbit becomes unstable via a torus bifurcation at  $\delta_r = -4.92^\circ$  and GTM\_sol is attracted back to the steep spiral dynamics of regime C. However, if the spin is to the left (i.e. with negative lateral variables) then, as the rudder is reduced back to zero, GTM\_sol remains attracted to the periodic orbit solutions and at  $\delta_r \approx 0^\circ$  the periodic orbit is that of dynamic regime F (for  $\delta_r = 0.009, \delta_e = -30$ ) in Fig. 2 (we note that, as  $\delta_r$  varies from  $> 20^\circ$  back towards  $0^\circ$ , the period-one orbit does become unstable for  $1^\circ \leq \delta_r \leq 4^\circ$ ; however, the resulting period-doubled orbits are stable). This confirms the earlier finding in Sec. IV B that the oscillatory spins only exist at zero aileron and rudder to the left with negative roll rates.

To further visualise this transition, Fig. 11 shows the results of a 50s time history which started on the steep spiral equilibrium of regime C where  $\delta_r = 0.009^\circ$ ,  $\delta_e = -30$ ,  $\alpha = 20.74^\circ$ ,  $p = 59.57^\circ/s$ , labelled point  $c$  in Fig. 10; then anti-spin (positive) rudder inputs were applied to try to counter the right steep spiral — see panel (d4) of Fig. 11. As expected from Fig. 10, once the rudder deflection exceeds  $\delta_r \approx 20^\circ$ , instead of countering the steep spiral, the rudder inputs actually induce the oscillatory spin of dynamics regime F. Once in this spin, if rudder deflection is decreased back to zero then instead of returning to the spiral, the aircraft stays in the oscillatory spin to the left and tracks back down to the oscillation between  $F_{min}$  and  $F_{max}$  in Fig. 2 once  $\delta_r = 0.009$ . Figure 12 shows the trajectory plot of the time history shown in Fig. 11. Such a time history simulation



**Fig. 10** One-parameter bifurcation diagrams in rudder deflection,  $\delta_r$ , of equilibrium and periodic solutions for GTM\_80l showing angle of attack  $\alpha$  (a) and roll rate  $p$  (b); here  $\delta_a = -0.004^\circ$ ,  $\delta_e = -30^\circ$  and  $\delta_t = 22.05\%$ .



**Fig. 11** Time history of the mechanism for entering the period-one spin of regime F from the steep spiral or regime C, showing time traces of:  $\alpha, \beta, V, p, q$  and  $r$  (panels a1—a6). Panels (b) and (c) show the corresponding trajectory in the  $(\beta, \alpha)$  and  $(\phi, \theta)$ -planes, respectively; the control surface schedules are: elevator, aileron, throttle and rudder (panels d1—d4).

is overlaid on top of the bifurcation diagram shown in Fig.13. This time history uses the same

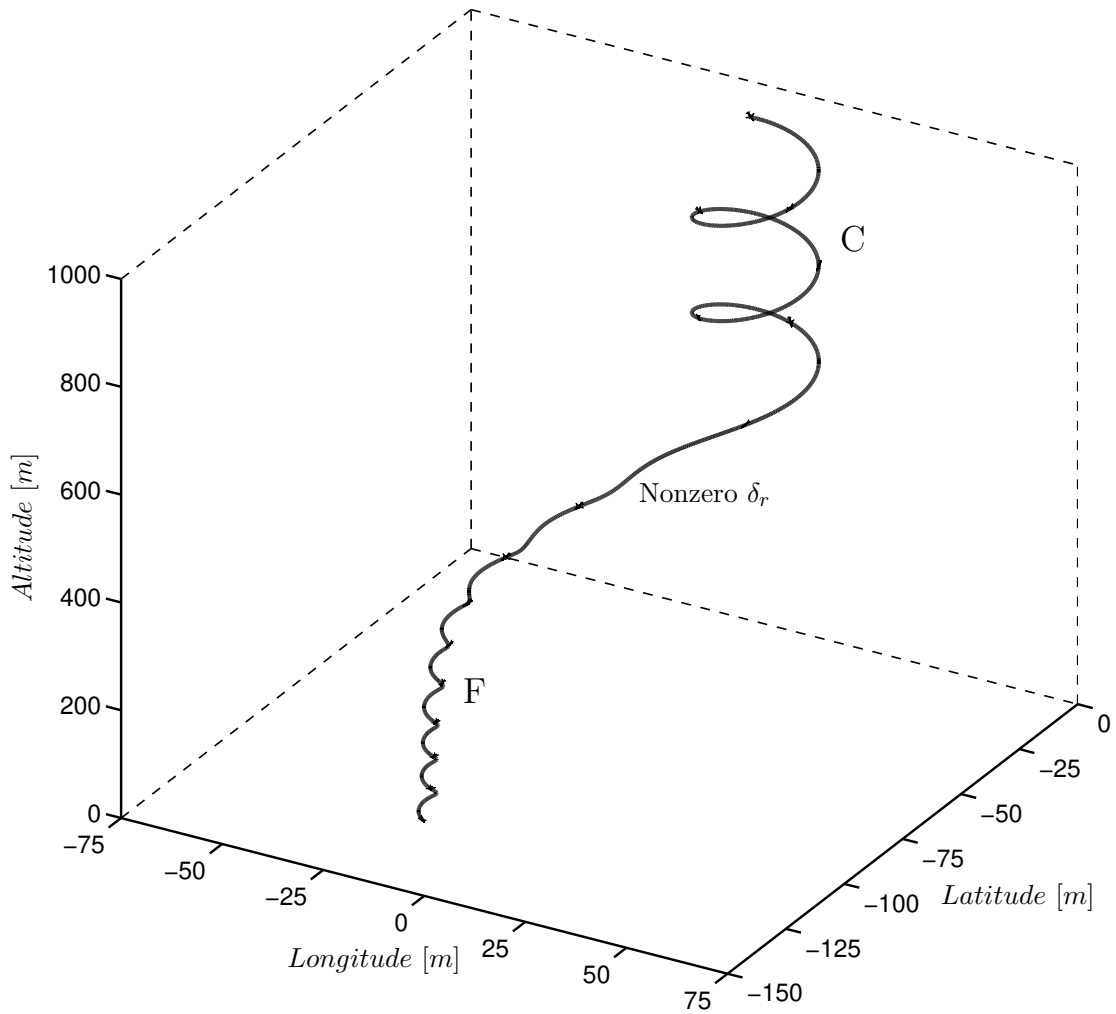


**Fig. 12** Trajectory of the time history from Fig. 11 showing the mechanism for entering the period-one spin of regime F from the steep spiral of regime C.

control surface amplitudes as in Fig. 11 but with a slower ramp input, at one tenth of the gradient, for better visualisation. Figures 11-13 demonstrate that applying rudder to get out of the spiral is an incorrect strategy for recovery from the upset and will actually increase the severity. On the other hand, simply pushing forward on the stick, increasing  $\delta_e$  to above  $\delta_e = -1.3^\circ$  and back into dynamics regime A, as described in section IV, will recover the aircraft from both the spiral of regime C or the oscillatory spins of regime F and G (passing through regime C before reaching regime A)—given sufficient altitude. This emphasises the advice given in Ref [7] that the first action for recovery should be to push forward on the stick and reducing angle of attack before trying to recover attitude.

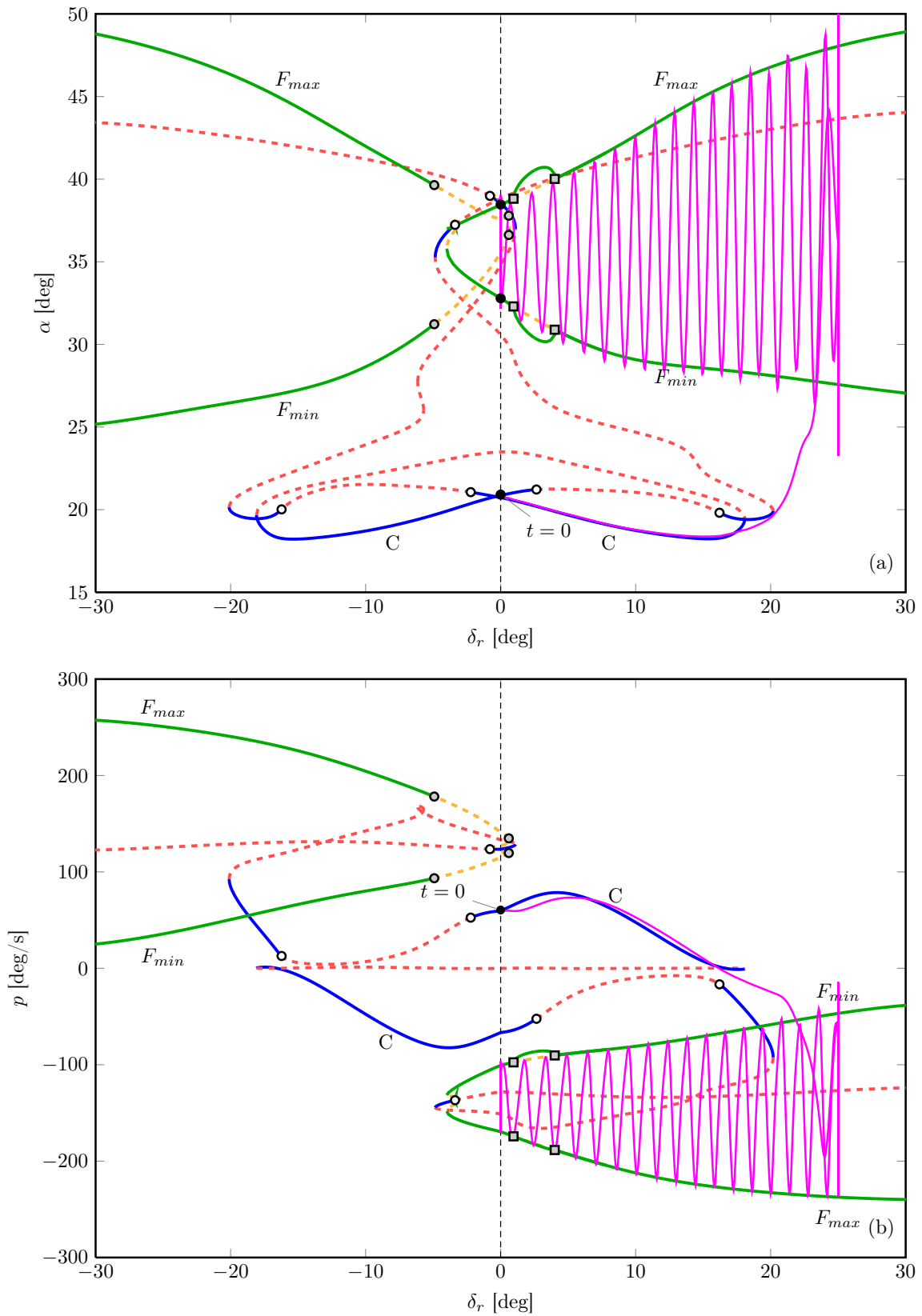


Fig. 13 One-parameter bifurcation diagrams in rudder deflection,  $\delta_r$ , of equilibrium and periodic solutions with a time history simulation overlaid for GTM\_80l, showing angle of attack  $\alpha$  (a) and roll rate  $p$  (b); here  $\delta_a = -0.004^\circ$ ,  $\delta_e = -30^\circ$  and  $\delta_t = 22.05\%$ .

## VI. Conclusion

The bifurcation analysis presented here has identified some of the rich variety of conditions governing the behaviour of the GTM; more specifically, it has found a number of stable attractors which are associated with upset. Indeed, compared to simulations that require one to wait for time history transients to disappear on weak attractors, bifurcation diagrams are much less computationally costly to create. Furthermore, bifurcation diagrams yield the underlying structure of the dynamical system and, hence, suggest where and when time histories should be run to further explain the predicted behaviour. Time history simulations have been presented to complement the bifurcation diagrams to give further clarity on the nature of the different regimes of attractor dynamics. It is shown that the GTM is susceptible to upset in the form of steep spiral motions, brought about by loss of spiral mode stability. The bifurcation analysis was also able to identify that rudder input aimed at reducing the steep spiral yaw rate can instead lead to oscillatory spin behaviour instead of recovery, and that recovery can be effected by returning the elevator setting to conventional trim values.

The approach taken in this paper is amenable to a number of extensions. Firstly, the open-loop behaviour of the GTM may be further explored by expanding the parameter space considered: this may involve additional control inputs and also variables such as centre of gravity location and parameters governing the damage scenarios that are incorporated into the model. Another potentially fruitful extension is to exploit bifurcation analysis techniques in considering the upset tendencies of the GTM augmented with closed loop control, and their potential to provide insight into control law design for upset prevention and recovery.

## Acknowledgments

This research is supported by an Engineering and Physical Sciences Research Council (EPSRC) award in collaboration with Airbus. We are grateful to members of the NASA's Langley Flight Dynamics Branch and Dynamics Systems and Control Branch for provision of the GTM model and advice on its use and flight characteristics. Discussions with Simon Pauck and Japie Engelbrecht from Stellenbosch University on implementation of the model are much appreciated.

## References

- [1] Chatrenet, D., “Air Transport Safety - Technology and Training,” *ETP 2010*, 2010, URL: [http://ec.europa.eu/invest-in-research/pdf/workshop/chatrenet%20\\_b3.pdf](http://ec.europa.eu/invest-in-research/pdf/workshop/chatrenet%20_b3.pdf) [cited 12 March 2013].
- [2] Aviation Safety Boeing Commercial Airplanes, “Statistical Summary of Commercial Jet Airplane Accidents Worldwide Operations 1959 - 2011,” Tech. rep., Boeing Commercial Airplanes, 2012.
- [3] “Airline Safety and Federal Aviation Administration Extension Act of 2010,” Public Law 111-216, Section 208, 2010.
- [4] Tarnowski, E., “Training Philosophy For Protected Aircraft in Emergency Situations,” *FAST Airbus Technical Digest*, No. 23, 1998, pp. 2–9,  
URL: [http://www.airbus.com/support/publications/?eID=dam\\_frontend\\_push&docID=17429](http://www.airbus.com/support/publications/?eID=dam_frontend_push&docID=17429) [cited 18 March 2013].
- [5] Gingras, D. R., Barnhart, B., Ranaudo, R., Martos, B., Ratvasky, T. P., and Morelli, E., “Development and Implementation of a Model-Driven Envelope Protection System for In-Flight Ice Contamination,” *AIAA Guidance, Navigation and Control Conference*, No. AIAA-2010-8141, 2010  
doi: 10.2514/6.2010-8141.
- [6] Dutoi, B. C., Richards, N. D., Gandhi, N., Ward, D. G., and Leonard, J. R., “Hybrid Robust Control and Reinforcement Learning for Optimal Upset Recovery,” *AIAA Guidance, Navigation and Control Conference and Exhibit*, No. AIAA-2008-6502, 2008  
doi: 10.2514/6.2008-6502.
- [7] Carbaugh, D. and Rockliff, L., “The Airplane Upset Recovery Training Aid, Revision 2,” 2008, URL: <http://flightsafety.org/archives-and-resources/airplane-upset-recovery-training-aid> [cited 12 March 2013].
- [8] Combs, S. R., Gousman, K. G., and Tauke, G. J., “Pilot activated automatic recovery system on the F-117A,” *1992 AIAA Aerospace Design Conference*, No. AIAA-1992-1126, 1992  
doi: 10.2514/6.1992-1126.
- [9] Advani, S. and Field, J., “Upset Prevention and Recovery Training in Flight Simulators,” *AIAA Modeling and Simulation Technologies Conference*, No. AIAA-2011-6698, 2011  
doi: 10.2514/6.2011-6698.
- [10] Fucke, L., Biryukov, V., Grigorev, M., Rogozin, V., Groen, E., Wentink, M., Field, J., Soemarwoto, B., Abramov, N., Goman, M., and Khrabrov, A., “Developing Scenarios for Research into Upset Recovery Simulation,” *AIAA Modeling and Simulation Technologies Conference*, No. AIAA-2010-7794, 2010  
doi: 10.2514/6.2010-7794.



- [11] Foster, J. V., Cunningham, K., Fremaux, C. M., Shah, G. H., and Robert A. Rivers, E. C. S., Wilborn, J. E., and Gato, W., “Dynamics Modeling and Simulation of Large Transport Airplanes in Upset Conditions,” *AIAA Guidance, Navigation, and Control Conference and Exhibit*, No. AIAA-2005-5933, 2005  
doi: 10.2514/6.2005-5933.
- [12] Jordan, T. L., Foster, J. V., Bailey, R. M., and Belcastro, C. M., “AirSTAR: A UAV Platform for Flight Dynamics and Control System Testing,” *25th AIAA Aerodynamic Measurement Technology and Ground Testing Conference*, No. AIAA-2006-3307, 2006  
doi: 10.2514/6.2006-3307.
- [13] Gregory, I. M., Cao, C., Xargay, E., Hovakimyan, N., and Zou, X., “L1 Adaptive Control Design for NASA AirSTAR Flight Test Vehicle,” *AIAA Guidance, Navigation, and Control Conference*, No. AIAA-2009-5738, 2009  
doi: 10.2514/6.2009-5738.
- [14] Crespo, L. G., Matsutani, M., and Annaswamy, A. M., “Design of an Adaptive Controller for a Remotely Operated Air Vehicle,” *Journal of Guidance, Control, and Dynamics*, Vol. 35, No. 2, 2012, pp. 406–422  
doi: 10.2514/1.54779.
- [15] Belcastro, C. M. and Jacobson, S. R., “Future Integrated Systems Concept for Preventing Aircraft Loss-of-Control Accidents,” *AIAA Guidance, Navigation, and Control Conference*, No. AIAA-2010-8142, 2010  
doi: 10.2514/6.2010-8142.
- [16] Carroll, J. V. and Mehra, R. K., “Bifurcation Analysis of Nonlinear Aircraft Dynamics,” *Journal of Guidance, Control, and Dynamics*, Vol. 5, No. 5, 1982, pp. 529–536  
doi: 10.2514/3.56198.
- [17] Zagaynov, G. I. and Goman, M. G., “Bifurcation analysis of Critical Aircraft Regimes,” *ICAS Paper*, No. 1CAS-80-4.2.1, 1984.
- [18] Guicheteau, P., “Bifurcation Theory in Flight Dynamics: An Application to Real Combat Aircraft,” *ICAS Paper*, No. ICAS-90-5.10.4, 1990.
- [19] Jahnke, C. and Culick, F., “Application of bifurcation theory to the high-angle-of-attack dynamics of the F-14,” *Journal of Aircraft*, Vol. 31, No. 1, 1994, pp. 26–34  
doi: 10.2514/3.46451.
- [20] Baghdadi, N. M., Lowenberg, M. H., and Isikveren, A. T., “Analysis of Flexible Aircraft Dynamics Using Bifurcation Methods,” *Journal of Guidance, Control, and Dynamics*, Vol. 34, No. 3, 2011, pp. 795–809

- doi: 10.2514/1.5146.
- [21] Planeaux, J. B., Beck, J. A., and Baumann, D. D., “Bifurcation analysis of a model fighter aircraft with control augmentation,” *AIAA Atmospheric Flight Mechanics Conference*, No. AIAA-1990-2836, 1990  
doi: 10.2514/6.1990-2836.
- [22] Avanzini, G. and Matteis, G. D., “Bifurcation Analysis of a Highly Augmented Aircraft Model,” *Journal of Guidance, Control, and Dynamics*, Vol. 20, No. 4, 1997, pp. 754–759  
doi: 10.2514/2.4108.
- [23] Goman, M. and Khramtsovsky, A., “Application of continuation and bifurcation methods to the design of control systems,” *Phil. Trans. R. Soc. Lon. A*, Vol. 356, No. 1745, 1998, pp. 2277–2295  
doi: 10.1098/rsta.1998.0274.
- [24] Liebst, B. S., “The dynamics, prediction, and control of wing rock in high-performance aircraft,” *Phil. Trans. R. Soc. Lon. A*, Vol. 356, No. 1745, 1998, pp. 2257–2276  
doi: 10.1098/rsta.1998.0273.
- [25] Goman, M. G., Zagainov, G. I., and Khramtsovsky, A. V., “Application of Bifurcation Methods to Nonlinear Flight Dynamics Problems,” *Progress in Aerospace Sciences*, Vol. 33, No. 9-10, 1997, pp. 539–586  
doi: 10.1016/S0376-0421(97)00001-83.
- [26] Macmillen, F. B. J. and Thompson, J. M. T., “Bifurcation analysis in the flight dynamics design process? A view from the aircraft industry,” *Phil. Trans. R. Soc. Lon. A*, Vol. Vol. 356, No. 1745, 1998, pp. 2321–2333  
doi: 10.1098/rsta.1998.0276.
- [27] Paranjape, A. A., Sinha, N. K., and Ananthkrishnan, N., “Use of Bifurcation and Continuation Methods for Aircraft Trim and Stability Analysis - A State-of-the-Art,” *Journal of Aerospace Sciences and Technologies*, Vol. 60, No. 2, 2008, pp. 85–100.
- [28] Kwatny, H. G., Dongmo, J.-E. T., Chang, B.-C., Bajpai, G., Yasar, M., and Belcastro, C., “Nonlinear Analysis of Aircraft Loss of Control,” *Journal of Guidance, Control, and Dynamics*, Vol. 36, No. 1, 2013, pp. 149–162  
doi: 10.2514/1.56948.
- [29] Dongmo, J.-E. T., “Aircraft Stall Recovery Using Nonlinear Smooth Feedback Regulators With Inputs Constraints,” *AIAA Guidance, Navigation, and Control Conference*, No. AIAA-2011-6303, 2011  
doi: 10.2514/6.2011-6303.
- [30] Pauck, S. J. and Engelbrecht, J. A. A., “Bifurcation Analysis of the Generic Transport Model with a

- view to Upset Recovery,” *AIAA Atmospheric Flight Mechanics Conference*, No. AIAA-2012-4646, 2012  
doi: 10.2514/6.2012-4646.
- [31] Engelbrecht, J. A. A., Pauck, S. J., and Peddle, I. K., “Bifurcation Analysis and Simulation of Stall and Spin Recovery for Large Transport Aircraft,” *AIAA Atmospheric Flight Mechanics Conference*, No. AIAA-2012-4801, 2012  
doi: 10.2514/6.2012-4801.
- [32] Jung, D. W., *Integration of Control Allocation Methods in Bifurcation Analysis Framework*, Ph.D. thesis, University of Bristol, Bristol, UK.
- [33] Kolesnikov, E. and Goman, M., “Analysis of Aircraft Nonlinear Dynamics Using Non-Gradient Based Numerical Methods and Attainable Equilibrium Sets,” *AIAA Atmospheric Flight Mechanics Conference*, No. AIAA-2012-4406, 2012  
doi: 10.2514/6.2012-4406.
- [34] Murch, A. M. and Foster, J. V., “Recent NASA Research on Aerodynamic Modeling of Post-Stall and Spin Dynamics of Large Transport Airplanes,” *45th AIAA Aerospace Sciences Meeting and Exhibit*, No. AIAA-2007-463, 2007  
doi: 10.2514/6.2007-463.
- [35] Murch, A. M., *Aerodynamic Modeling of Post-Stall and Spin Dynamics of Large Transport Airplanes*, Master’s thesis, Georgia Institute of Technology, Atlanta, GA, 2007.
- [36] Gill, S. J., Lowenberg, M. H., Krauskopf, B., Puyou, G., and Coetzee, E., “Bifurcation Analysis of the NASA GTM with a View to Upset Recovery,” *AIAA Atmospheric Flight Mechanics Conference*, No. AIAA-2012-4648, 2012  
doi: 10.2514/6.2012-4648.
- [37] Kuznetsov, Y. A., *Elements of Applied Bifurcation Theory Third Edition*, Vol. 112 of *Applied Mathematical Sciences*, Springer-Verlag New York, Inc., 175 Fifth Avenue, New York, NY 10010 USA, 2004.
- [38] Krauskopf, B., Osinga, H. M., and Galán-Vioque, J., *Numerical Continuation Methods for Dynamical Systems: Path following and boundary value problems*, No. ISBN 978-1-4020-6355-8 in Understanding Complex Systems Series, Springer-Verlag New York, Inc., 175 Fifth Avenue, New York, NY 10010 USA, 2007.
- [39] Etkin, B., *Dynamics of Atmospheric Flight*, Chapter 5, J. Wiley and Sons, NJ, USA, 1972.
- [40] Doedel, E. J. and Oldeman Bart, E., “AUTO-07P: Continuation and Bifurcation Software for Ordinary Differential Equations,” 2009, Contributions by Alan R. Champneys, Fabio Dercole, Thomas Fairgrieve, Yuri Kuznetsov, Randy Paffenroth, Björn Sandstede, Xianjun Wang, Chenghai Zhang.

- [41] Rankin, J., Coetzee, E., Krauskopf, B., and Lowenberg, M., “Bifurcation and Stability Analysis of Aircraft Turning on the Ground,” *Journal of Guidance, Control, and Dynamics*, Vol. 32, No. 2, 2009, pp. 499–510  
doi: 10.2514/1.37763.
- [42] Thota, P., Krauskopf, B., and Lowenberg, M., “Interactions of Torsion and Lateral Bending in Aircraft Nose Landing Gear Shimmy,” *Nonlinear Dynamics*, Vol. 57, No. 3, 2008, pp. 455–467  
doi: 10.1007/s11071-008-9455-y.
- [43] Knowles, J. A. C., Krauskopf, B., and Lowenberg, M. H., “Numerical Continuation Applied to Landing Gear Mechanism Analysis,” *Journal of Aircraft*, Vol. 48, No. 4, 2011, pp. 1254–1262  
doi: 10.2514/1.C031247.
- [44] Jones, C., Lowenberg, M. H., and Richardson, T. S., “Tailored Dynamic Gain-Scheduled Control,” *Journal of Guidance, Control, and Dynamics*, Vol. 29, No. 6, 2006, pp. 1271–1281  
doi: 10.2514/1.17295.
- [45] Coetzee, E., Krauskopf, B., and Lowenberg, M., “The Dynamical Systems Toolbox: Integrating AUTO into Matlab,” *16th US National Congress of Theoretical and Applied Mechanics*, No. USNCTAM2010-827, US National Congress of Theoretical and Applied Mechanics, AIAA, 2010.
- [46] Morelli, E. A., “Global Nonlinear Aerodynamic Modeling Using Multivariate Orthogonal Functions,” *Journal of Aircraft*, Vol. 32, No. 2, 1995, pp. 270–277  
doi: 10.2514/3.46712.
- [47] Duke, E. L., Antoniewicz, R. F., and Krambeer, K. D., “Derivation and Definition of a Linear Aircraft Model,” 1988.
- [48] Murphy, P. C., Klein, V., and Frink, N. T., “Unsteady Aerodynamic Modeling in Roll for the NASA Generic Transport Model,” *AIAA Atmospheric Flight Mechanics Conference*, No. AIAA-2012-4652, 2012  
doi: 10.2514/6.2012-4652.